https://doi.org/10.5194/se-2020-75
Preprint. Discussion started: 27 May 2020

Solid Earth Discussions

Water- and land-borne geophysical surveys before and after the sudden water-level decrease of two large karst lakes in southern Mexico

Matthias Bücker[1,2], Adrián Flores Orozco[2], Jakob Gallistl[2], Matthias Steiner[2], Lukas Aigner[2], Johannes Hoppenbrock[1], Ruth Glebe[1], Wendy Morales Barrera[3], Carlos Pita de la Paz[4], Emilio García García[4], José Alberto Razo Pérez[4], Johannes Buckel[1], Andreas Hördt[1], Antje Schwalb[5], Liseth Perez[3,5]

1Institute for Geophysics and Extraterrestrial Physics, TU Braunschweig, Braunschweig, 38106, Germany.
2Department of Geodesy and Geoinformation, Research Group Geophysics, TU Wien, 1040, Austria.
3Instituto de Geología, Universidad Nacional Autónoma de México, Mexico City, 04510, Mexico.
4Geotem Ingeniería S.A. de C.V., Mexico City, 14640, Mexico.
5Institute of Geosystems and Bioindication, TU Braunschweig, 38106, Germany.

Correspondence to: Matthias Bücker, (m.buecker@tu-braunschweig.de)

Abstract. The present geophysical study was motivated by the need to determine suitable coring locations for paleolimnological studies in two karst lakes (Metzabok and Tzibaná) of the Lacandon Forest in Chiapas, southern Mexico. We used seismic and transient electromagnetic methods to map the sediment thickness below the lake floor. When lakes were filled in March 2018, we collected seismic data with a sub-bottom profiler (SBP) and transient electromagnetic (TEM) data with a floating single-loop configuration. The latter aimed at assessing the TEM method as an alternative to seismic methods for the investigation of lake sediments and geology. After the first campaign, water levels of both studied lakes dropped dramatically by July 2019, leaving Lake Metzabok (maximum depth ~25 m) dry and Lake Tzibaná (~70 m) with a water level decreased by approx. 30 m. After the sudden drainage of the lakes, we complemented water-borne measurements by a survey carried out on the exposed lake floor in October 2019, when lake levels were still low. During this second campaign, we collected time-domain induced polarization (TDIP), and seismic refraction tomography (SRT) data on the desiccated bed of Lake Metzabok and some dry parts of Lake Tzibaná. By comparing the various data sets, we find that (i) SBP and TDIP phase images consistently resolve the thickness of the fine-grained lacustrine sediments covering the lake floor, (ii) TEM and TDIP resistivity images consistently detect the upper limit of the limestone bedrock and the geometry of fluvial deposits of a river delta, and (iii) TDIP and SRT images suggest the existence of a layer that separates the lacustrine sediments from the limestone bedrock and consists of collapse debris mixed with lacustrine sediments. While our results do not imply that resistivity-based methods could generally replace seismic reflection surveys for lake-bottom reconnaissance, they clearly show that TEM and TDIP surveys can provide important complementary information and resolve additional geological units or bedrock heterogeneities.

https://doi.org/10.5194/se-2020-75
Preprint. Discussion started: 27 May 2020

1 Introduction

Lake sediments are important archives of freshwater and terrestrial environmental information and in particular sediment cores can be used to reconstruct past climate and ecological changes (Cohen, 2003; Schindler, 2009). The northern neotropical region hosts a large number of lakes of different origins (karst, volcanic, maar, tectonic) (Pérez et al., 2011; Sigala et al., 2017). Recent studies have highlighted the great potential of sedimentary sequences from lakes in Mexico and Guatemala as continuous paleoenvironmental and paleoclimatic records during the late Quaternary (Díaz et al., 2017; Lozano et al, 2017; Cohuo et al., 2018). To identify suitable drilling locations providing continuous paleoenvironmental records at a high temporal resolution, knowledge about sediment thickness and composition, depth to bedrock, and possible heterogeneities within the lake sediments is needed (Last and Smol, 2002). Geophysical methods can efficiently provide such information from the local scale up to the lake-basin scale.

Due to the usually sharp contrast between seismic velocities of sediment layers and the underlying bedrock, (reflection-) seismic methods are often given priority over other geophysical methods for lake-bottom reconnaissance (Scholz, 2002). In particular, low-frequency echo sounders (e.g., Dondurur, 2018), also referred to as sub-bottom profilers (SBP), allow to quickly map sediment deposits of several tens of meters based on single-channel seismic data. Nevertheless, electrical-resistivity data provided by electrical resistivity tomography (e.g., Binley and Kemna, 2005) or electromagnetic soundings (e.g., Kaufman et al., 2014) can complement the mostly geometrical information obtained from reflection-seismic or sub-bottom profiling measurements (Butler, 2009). Under certain conditions such as high lake-bed reflectivity and/or low reflectivity of targeted boundaries, seismic methods may, however, provide insufficient results and therefore alternative methods are needed.

Recent studies using direct-current (DC) electrical resistivity for water-borne investigations on freshwater bodies include surveys with floating (e.g., Befus et al., 2012; Orlando, 2013; Colombero et al., 2014) or underwater electrode chains (e.g., Toran et al., 2015) and provide evidence for the potential of this method for shallow-water applications. Electrical resistivity can also be assessed by electromagnetic methods, which, compared to DC resistivity measurements, offer a more compact experimental layout. Electromagnetic surveys are often carried out as transient electromagnetic soundings with floating magnetic sources and receivers. Hatch et al. (2010), for example, used an in-loop configuration with a ~7.5 m x 7.5 m transmitter and a ~2.5 m x 2.5 m receiver to map river bed salinization in an Australian river with an average water depth of 5-10 m. Mollidor et al. (2013) used a similar but slightly larger setup (~18 m x 18 m transmitter, ~6 m x 6 m receiver) to map a thick conductive sediment layer below the bottom of a 20-m deep maar lake in Germany. Some older relevant case studies with shallow-water applications of both techniques, DC resistivity and electromagnetic soundings, were reviewed by Butler (2009).

In a previous study, we successfully used geoelectrical and electromagnetic methods to investigate the sedimentary infill of two desiccated lakes (Bücker et al., 2017). Here, we add a systematic field study that assesses the potential of water-borne resistivity-based methods to complement seismic methods for the investigation of water-filled lakes. The basic assumption behind this approach is that a (sufficiently thick) layer of fine-grained lakebed sediments would be more conductive than the

https://doi.org/10.5194/se-2020-75
Preprint. Discussion started: 27 May 2020

underlying bedrock and the water column and thus detectable by resistivity-based methods. Because applications of transient electromagnetic (TEM) soundings on lakes are still rare, in this study, we are particularly interested in the evaluation of such water-borne measurements.

When the lakes were filled, we collected seismic data with a SBP and TEM soundings to assess the electrical resistivity of the lake bottom. As we used floating experimental setups for both methods, device and targeted sediment layer on the lake bottom were often separated by a water column of 20 m and more, with the corresponding limiting effect on the resolution of the sediment-thickness estimates. The sudden and unexpected drainage of the investigated karst lakes, which occurred only a few months after the water-borne survey, provided us with the unique opportunity to collect reference data directly on the dry lake bed. Seismic reference data was collected with a seismic refraction tomographic (SRT) setup in order to provide information on both refractor geometry and seismic velocities of the different geophysical units. Electrical reference data was measured with the time-domain induced polarization (TDIP) method, which has fewer limitations regarding the detectability of thin near-surface layers and heterogeneities than the transient electromagnetic method. Furthermore, the polarization properties of the subsurface materials assessed by TDIP measurements provide additional information and can improve the interpretation of TEM and ERT results.

2 Study area

The study area is located in the Lacandon Forest (16°–17.5° N; 90.5°–92° W; 500–1500 m.a.s.l.), which occupies the north-eastern part of the State of Chiapas, Mexico. The region belongs to the Chiapas fold belt with its WNW-trending folds and thrusts (Fig. 1), which mainly developed in massive cretaceous limestone (García-Gil and Lugo Hupb, 1992). The orogeny of the Chiapas fold belt is related to the collision of the Tehuantepec Transform/Ridge on the Cocos plate with the Middle America Trench during the Middle Miocene (Mandujano-Velazquez and Keppie, 2009). The resulting anticlines and synclines dominate the topography in the study area forming long WNW-directed valleys and mountain ranges. The tectonically fractured limestone geology, in conjunction with the humid subtropical climate, favour an intensive karstification (García-Gil and Lugo Hupb, 1992). In the valleys, lakes formed by bedrock dissolution, such as dolines (or sinkholes), uvalas (formed by two or more dolines) and poljes (larger karst depressions), are mostly aligned in the main fold direction.

The lake system of Metzabok (17°6'30"–17° 8'30" N, 91°36'30"– 91°38'50" W, ~550 m a.s.l.) consists of 21 lakes of different sizes, the majority of which are interconnected when water levels are high (Lozada Toledo, 2013). The two largest lakes of the system are Lake Tzibaná (area 1.24 km²; max. depth 70 m) and Lake Metzabok (0.83 km²; 25 m) (see Fig. 1). The river Nahá is the principal superficial tributary connecting the lake system of Metzabok with the one of Nahá (~830 m a.s.l.); a superficial outlet of the lake system does not exist. Although the (additional) water supply and discharge through the underlying karst system is unknown, fast lake-level changes indicate a dominant role of subsurface hydrology. Usually, seasonal lake-level changes amount to ~10 m and can be traced back to prehispanic times (Lozada Toledo, 2013). Between March and August

https://doi.org/10.5194/se-2020-75
Preprint. Discussion started: 27 May 2020

95 2019 an extreme lake-level drop occurred that left Lake Metzabok completely dry and decreased the water level of Lake Tzibaná by ~30 m.

3 Data acquisition and processing

With the overall goal of mapping sediment thicknesses below the lake floor of various lakes of the karst lake systems of Metzabok and Nahá, we carried out a first geophysical campaign employing seismic (SBP) and TEM methods, when lake
100 levels were maximum in March 2018 (Fig. 2a). Immediately after the dramatic lake-level decline, we revisited the study site in October 2019 to collect refraction seismic tomography (SRT) data and perform TDIP measurements directly on the dry lake bottom (Fig. 2a, b).

3.1 Electrical resistivity measurements in the laboratory

In October 2019, a total of six surface sediment samples (top 10 cm) and two water samples were collected at different locations
105 for laboratory analyses (see sampling locations in Fig. 2a, b). On the dry lake bottom, sediment samples were collected using a small spade, whereas an Ekman grab sampler was used to retrieve sediment samples from water-covered areas. Sediment samples were stored in sealed plastic bags in order to prevent the loss of moisture; water samples were stored in plastic bottles. All samples were kept cool during transport and storage in order to prevent an increased degradation of organic matter. The electrical conductivity of the water samples (at 20°C) was measured with a laboratory probe. The frequency-dependent
110 complex electrical resistivity of the samples was measured using a Chameleon I measuring device (Radic Research) in the frequency range from 1 mHz to 240 kHz. To this end, the unconsolidated sediments were filled into four-point measuring cells with non-polarizing potential electrodes as used by Kruschwitz (2007) and Bairlein et al. (2014). Prior to and during the measurement, the measuring cell was stored in a climate chamber to keep the sample at a constant temperature of 20°C. Measurements were repeated over a period of 4 to 5 days after filling the cell and inserting it into the climate chamber in order
115 to assure equilibrium conditions in the sample. Measurements on relatively dry samples (MET19-A and TSI19-A) resulted in comparably high phase values. These samples were removed from the measuring cell, saturated with water of the corresponding lake (using one of the two water samples), and filled again into the measuring cell. This procedure led to more consistent phase measurements compared to the other samples.

3.2 Collection of sub-bottom profiler (SBP) lines

120 Low-frequency echo-sounders, often referred to as sub-bottom profilers (SBP), are single channel seismic reflection systems, which are used to obtain bathymetric profiles and provide a high-resolution stratigraphic display of the uppermost sediments (e.g., Dondurur, 2018). In March 2018, SBP lines were collected with the 10-kHz transducer StrataBox HD (SyQwest) mounted on a motor boat. Data was recorded with a record length of 200 ms and a 1024 Hz sampling frequency. The SBP device was mounted mid-ships in a side mount configuration, with the transducer positioned at 0.4 m below the water surface.

https://doi.org/10.5194/se-2020-75
Preprint. Discussion started: 27 May 2020

Prior to each survey, the acoustic wave velocity profiles of the water columns of the two studied lakes were measured with a Digibar S (Odom Hydrographic). SBP lines were laid out in a regular NS- and EW-oriented grid with separations of 100 m and 300 m, respectively (see Fig. 1). Navigation data was measured with a differential GPS and stored along with the SBP data.

During processing, the SBP acoustic traces were read in using code provided by Kozola (2020) and visualized using a Matlab script available with this manuscript. The average values of the acoustic wave velocity of the water columns (1486.6 m/s for both lakes) were used to convert the two-way travel time of the acoustic pulse into a depth scale for the seismic profiles.

3.3 Transient electromagnetic (TEM) soundings

Transient electromagnetic (TEM) soundings were carried out from the water surface using a single-loop configuration in March 2018. The loop with a diameter of 22.9 m (surface area: ~412 m²) consisted of a single, insulated copper wire attached to a floating ring made of twenty-four 1-inch PVC tubes. The ring was towed by an inflatable boat, where it was connected to the measuring device, a TEM-FAST48 (manufactured by Applied Electromagnetic Research). During the measurements, the loop was separated by 5 m from the inflatable boat. A simple echo-sounder (Garmin Fishfinder series) was used to measure the water depth at each sounding site. For the acquisition of TEM sounding data, we used a transmitter current of 1 A, and 3328 transients were stacked at each sounding site within 32 time gates between 3.6 µs and 1024 µs after current shut-off. Due to the comparably low measurement velocity (ca. 3 min per sounding) and the poor maneuverability of the experimental setup, TEM data was acquired along a limited number of irregularly distributed lines of interest (Fig. 2a).

During the processing, all transients were truncated to times from 20 to 200 µs and inverted using the software ZondTEM1d (Kaminsky, personal communication). A smoothness-constrained modelling approach was used to obtain a one-dimensional multilayer model for each sounding site separately. The water depth measured with the echo-sounder was used as a-priori information by fixing the thickness of the first layer to this value. The electrical resistivity of the water layer was fixed to 25 Ωm. This value was manually adjusted to provide a good overall fit for all soundings. Especially for sites with shallow water depths and a resistive lake bed (i.e., bedrock not covered by conductive sediments), constraining the resistivity of the water layer significantly improved the imaging results.

3.4 Time-domain induced polarization (TDIP)

Time-domain induced polarization (TDIP) data was acquired with a SyscalPro Switch 48 device (IRIS Instruments) using 48 stainless-steel electrodes separated by 5 m or 10 m depending on the target. The soft and wet mud on the exposed lakebed provided a good contact between electrodes and ground. Where TDIP profiles crossed limestone outcrops, electrodes were inserted into sediment-filled fractures in order to keep contact resistances as low as possible. Measurements were carried out with injection currents between 0.5 A and 1 A, one single stack and a 50% duty cycle with 500 ms pulse length (i.e., duration of off time is also 500 ms). After an initial delay of 20 ms after current shut off, the voltage decay was sampled in 20 time windows with a constant length of 20 ms. We used a dipole-dipole configuration combining short dipole lengths of one

https://doi.org/10.5194/se-2020-75
Preprint. Discussion started: 27 May 2020

electrode spacing (skip-0) for superficial measurements with longer dipole lengths of two and four times the electrode spacing (skip-1 and skip-3) for moderate and large depths, respectively. To prevent loss of data quality due to remnant electrode polarization, the measurement protocol avoids potential readings using electrodes that had been used as current electrodes before (Dahlin et al., 2002). TDIP lines of varying length were laid out along (and parallel to) selected 2018 SBP and TEM lines on both lakes (Fig. 2a, b). In order to cover the full length of the north-south running SBP line L4 NS, TDIP lines MET19-1 and MET19-2 were carried out as a roll-along profile with an electrode spacing of 10 m and an overlap of 12 electrodes.

During the processing, we removed erroneous measurements defined as those associated with negative apparent resistivity and/or integral chargeability readings (Flores Orozco et al., 2018). After the removal of erroneous measurements, raw-data pseudo sections were inspected and additional outliers were defined as those readings with integral chargeability values above 6 mV/V. Integral chargeability values were linearly converted to frequency-domain phase shifts assuming a constant phase angle response (i.e., no frequency dependence) following the approach outlined by Van Voorhis et al. (1973) and implemented by Kemna et al. (1999). 2D complex-resistivity sections were then reconstructed from the filtered data using the smoothness-constrained least-squares algorithm CRTomo (Kemna, 2000).

3.5 Seismic refraction tomography (SRT)

Seismic-refraction tomography (SRT) data was acquired with the 24-channel seismograph Geode (Geometrics) and twenty-four 28-Hz geophones installed along a line at 5 m spacing in October 2019. To generate the seismic signal, a 7.5 kg sledgehammer hitting a steel plate was used at 25 shot points between the geophone positions as well as at distances of 2.5 m from the first and last geophone, respectively. At each shot point, five shots were stacked. Due to the limited length (115 m between the first and the last geophone) and investigation depth, SRT data was only collected in the central parts of selected TDIP profiles (Fig. 2a, b).

Based on the first-arrival travel times, a tomographic inversion scheme determines the two-dimensional velocity structure below the SRT profile (e.g., White, 1989). For the picking of the first arrivals, we used a Python toolbox developed at the TU-Wien. The observed travel times were then inverted with the pyGIMLi framework (Rücker et al., 2017) following a smoothness-constrained scheme. Due to the unconsolidated, muddy ground encountered on the lake floor, the signal-to-noise (S/N) ratio of the SRT data was challenging and lead to a low picking percentage, especially at larger offsets (distance between shot point and geophone location).

4 Results and interpretation

4.1 Laboratory measurements

The complex-resistivity measurements on the six sediment samples carried out in the laboratory (Figure 3) show that most resistivity values vary within a relatively narrow range between 10 and 15 Ωm. Only the resistivity of one sample (TSI19-A) from the river delta in Lake Tzibaná reached values between 18 and 20 Ωm. Figure 3b shows that phase values (here $-\varphi$) in the

https://doi.org/10.5194/se-2020-75
Preprint. Discussion started: 27 May 2020

frequency range from 1 to 10 Hz, which is mainly tested by our TDIP measurements, are roughly comprised between 0.5 and 4 mrad. Again, the only exception is sample TSI19-A with phase values of up to 6 mrad in the relevant frequency range. The elevated phase values at high (>1 kHz) frequencies are typical electromagnetic coupling effects (Pelton et al., 1978), but do not affect our TDIP measurements, due to the long initial delay before the sampling of the voltage decay starts.

The resistivity of the two water samples from the remaining water bodies used to improve the readings of two dry samples (MET19-A and TSI19-A) were 11.9 Ωm (Metzabok) and 26.8 Ωm (Tzibaná), respectively. They are significantly lower than the average water resistivity of ~34.5 Ωm reported by Rubio Sandoval (2019) for water samples collected from Lake Metzabok during high lake-level stands in 2016. This reduction of electrical resistivity (i.e., increase of conductivity) is probably due to the larger effect of evaporation on the salinity of small (and shallow) water bodies. Indeed, the remaining water body in Lake Metzabok was much smaller (~50 m²) than the one in Lake Tzibaná (~5000 m²).

The average resistivity of the sediment samples for the frequency range between 1 and 117 Hz (and excluding sample TSI19-A) is 12.25 Ωm, which is typical for saturated clayey sediments (e.g., Reynolds, 2011). Note that due to the contribution of surface conduction along the charged clay-mineral surfaces (Waxman and Smits, 1968), the bulk resistivity of the sediments is even lower than the average resistivity of 25-35 Ωm (during high lake-level stands). In our case, this resistivity contrast between lake water and sediments by a factor of 2 to 3 is of particular relevance as it allows us, in principle, to detect the two materials as separate units. To our best knowledge, this is the first time that the phase spectra of fresh lake-bed sediments have been measured in the laboratory.

4.2 Field measurements on Lake Metzabok

In October 2019, Lake Metzabok (average depth 15 m) was completely dry, except for some residual ponds. Its sediment-covered bottom is mostly flat with steep walls (>50% slope) and some cliffs along the shore line (Fig. 4a). Only some drainage channels, steep limestone hillocks, and small ponds (Fig. 4a–d) eventually disrupt the smooth lake-bottom topography.

4.2.1 Profile 1

The north-south oriented SBP line L4 NS on Profile 1 crosses various of these topographic elevations and depressions, which are well resolved by the first reflector in the seismogram (Fig. 4e). Within the depressions between the limestone outcrops, a second reflector, the geometry of which shows a certain consistency with the surface of the limestone outcrops, can be interpreted as the lower limit of the sediment cover. The SBP data clearly shows that not only the elevations (outcrops) but also the depressions in the sediment cover are influenced by the topography of the underlying limestone: Both depressions, the drainage channel in the northern as well as the small pond in the southern part, are associated with local heights in the limestone surface. Based on the SBP images, the sediment thickness mostly varies between 5 and 7 m along Profile 1.

Below the surface of the limestone outcrops and the lower limit of the sediment cover, respectively, we observe zones of diffuse reflectivity. These might be related to the heavily fractured and dissolved limestone. Particularly in the flat areas, the sediment cover might also be underlain by blocks of collapsed limestone with sediment filling the spaces between blocks and

https://doi.org/10.5194/se-2020-75
Preprint. Discussion started: 27 May 2020

debris. The lakes of the study area show all characteristics of karst lakes, which are expected to originate from collapsed karst cavities, and the collapse debris should still be present below the sediment cover.

The electrical images obtained from the co-located TDIP line (MET19-1 and 2) supports this interpretation: The resistivity image (Fig. 4f) shows a gross separation into two main units: The (i) sediments as well as the supposed limestone debris-sediment mixture stand out with low resistivity values between 10 and 20 Ωm, while the (ii) limestone outcrops and the deep part of the section are characterized by higher resistivity values of up to 300 Ωm. The phase image (Fig. 4f) also shows a separation into units with low and intermediate values. Here, a much thinner top layer (compared to the conducting layer in Fig. 4f) stands out with phase values between 0 and 5 mrad, while the limestone bedrock shows phase values >5 mrad. Due to the relatively low data cover after outlier-removal for large dipole separations, we do not interpret the phase values at depths >50 m.

For the sediment infill, both the resistivity values of 10-20 Ωm and the phase values below 5 mrad are in agreement with our laboratory measurements on the sediment samples of Lake Metzabok, corresponding to an average resistivity of ~12 Ωm and phase values (here $-\varphi$) < 4 mrad. In contrast, resistivity and phase values associated with the limestone bedrock are significantly higher than those of the fine-grained sediment cover. The intermediate layer, which we interpret as mixture of fine-grained sediments and the collapse debris, seems to inherit the low resistivity of the supposed clay-rich matrix, while the phase or polarization response is increased by the limestone debris.

4.2.2 Profile 2

The north-south oriented Profile 2 runs parallel to the last part of Profile 1 but shifted ~10 m East. It is centred at the small pond (Fig. 4d) and has a smaller electrode spacing (5 m instead of 10 m) to better resolve the sediment-limestone contact below the bottom of the pond. The electrical images (Fig. 5a, b) show the same characteristics as seen in the corresponding part of Profile 1. Due to the higher resolution, here, we observe an internal layering of the shallow conductive units with a less conductive (30-50 Ωm) top layer of ~10 m thickness and a more conductive (<20 Ωm) layer that extends down to 30 m in the northern and southern parts of the line. The separation into two units becomes much more obvious from the phase image, where the superficial layer is less polarizable (well below 4 mrad) than the deeper part. A few meters East of the centre of the profile, the resistive limestone bedrock crops out, which might explain the significantly increased resistivity (>100 Ωm) and phase values (>6 mrad) over the first 20 m of depth below this part of the profile.

The p-wave velocity structure in the SRT image (Fig. 5c) confirms the presence of these three units: The shallowest layer, corresponding with the sediment infill characterized by velocities between 200 and 1000 m/s, which is in agreement with values for unconsolidated fine-grained sediments reported in the literature (Uyanık, 2011). In the second layer, velocities increase to 1500-2000 m/s, and at depths between 15 and 20 m, a sudden increase to values >2500 m/s is observed. The p-wave velocities of the deepest unit agree with the lower limit of typical ranges for limestone (Reynolds, 2011), which can be explained by the high degree of fracturing and dissolution of the karst bedrock. The seismic velocities of the intermediate layer

https://doi.org/10.5194/se-2020-75
Preprint. Discussion started: 27 May 2020

do not provide any additional information on its nature, but could well be explained by limestone debris or heavily fractured and dissolved limestone with sediment-filled open spaces.

4.2.3 Profile 3

The comparison of the SBP line along the west-east directed Profile 3 with the corresponding electrical resistivity images (Fig. 6) confirms the interpretation of the electrical images: The step in the lower limit of the sediment layer around 490 m along the SBP profile, is also reflected in the resistivity structure and is clearly resolved in the phase image. Again, the conductive unit extends far below the SBP reflector, in particular between 440-490 m along the profile. As we interpret this reflector as the contact between pure sediments and the mixed sediment-collapse debris, this means that the mixed layer has a lower resistivity than the superficial fine-grained sediment layer. Along this profile, both sediment-bearing layers are characterized by low phase values. The sediment-covered limestone bedrock between 440 and 530 m is characterized by high phase values, while phase values decrease as this unit approaches the surface and crops out at the end of the profile. The low phase values of the limestone outcrop do not fit the previously stated general characteristics of this unit but might be related to variations in composition and/or degree of fracturing of the limestone bedrock.

4.2.4 Profile 4

Fig. 7a shows the electrical resistivity image reconstructed from 12 TEM soundings along the profile crossing Lake Metzabok from Northwest to Southeast. A conductive layer of varying thickness below the lake floor indicates the presence of fine-grained sediment infill across the entire basin. This layer only disappears close to the shoreline (i.e., towards the eastern end of the profile). Between stations MET3 and MET7, the TEM image recovers a resistivity distribution similar to the one of co-located TDIP profile (Fig. 7b). Taking into account that the water-borne TEM survey was carried out with an average of 15 m water column, the consistency with the TDIP resistivity results from the lakebed clearly indicates a high quality of the obtained TEM imaging results.

As observed before, the phase image (Fig. 7c) shows a non-polarizable top layer, which at a depth of ~10 m is underlain by a unit with a higher polarization response (absolute phase values around 10 mrad and higher), corresponding with the debris-sediment unit. The SRT tomogram (Fig. 7d) shows a sharp increase in p-wave velocity at depths between 20 m (in the western part) and 30 m (in the eastern part). This southeast-dipping surface correlates with a similar structure in the TDIP resistivity model, which we again interpret as the contact with the limestone bedrock.

4.2.5 Geological interpretation of the geophysical survey on Lake Metzabok

The schematic sketch presented in Fig. 8 summarizes our geological interpretation of the geophysical profiles of Lake Metzabok and the observations made on the exposed bed of the drained lake. It rests on the assumption that the lakes in the study area are formed by the coalescence of a number of dolines that resulted from the collapse of karst cavities. The remains of the collapsed limestone are expected to have formed a debris layer covering the floor of the former caves. Subsequently,

https://doi.org/10.5194/se-2020-75
Preprint. Discussion started: 27 May 2020

the fluvial input of fine-grained lake sediments has first filled up the interspaces between the blocks and then buried the collapse remains, forming the two uppermost units observed below all profiles.

Table 1 summarises the physical properties of the main units of this geological interpretation. The electrical resistivity of the fine-grained sediments and the mixed collapse debris and sediment layer is comprised within a relatively narrow range. In the TEM and TDIP resistivity images, these two units may appear as one conductive unit (see red dotted lines in Fig. 8). It is not clear, why the addition of the more resistive lime stone debris should decrease the resistivity of the mixed unit compared to the pure fine-grained sediments. In terms of the phase values, the distinction between these units is clearer and the increase of the phase values in the mixed layer is straightforward (because the limestone is more polarizable than the fine-grained sediments). The clearest indication of the inner structure of the conductive unit comes from the collocated SBP sections, which show a clear seismic reflector at the corresponding depth. The limestone bedrock becomes detectable by its high p-wave velocity in the SRT images and its high resistivity (TEM and TDIP), while its phase response varies over a larger range and is, thus not as unambiguous. It is worth mentioning that wherever the fine-grained sediments are underlain by the collapse debris layer, the limestone bedrock does not appear as an additional reflector in the SBP sections.

4.3 Field measurements on a river delta of Lake Tzibaná

Besides the measurements in the completely drained Lake Metzabok, we also present data from one profile crossing the delta of the Nahá river in the southern part of Lake Tzibaná. The survey layout and satellite image in Fig. 2b show that the land-borne measurements (i.e., TDIP and SRT) along this profile only covered those parts of the river delta, which were dry during October 2019.

In contrast to the well-sorted and mainly fine-grained sediments (clay/silt) on the mostly flat bed of Lake Metzabok, here, we expect a higher fraction of coarser material (sand/gravel) in the fluvial deposits. Indeed, the resistivity images of both TEM and TDIP measurements presented in Fig. 9a, b consistently show three main units: the resistive (>100 Ωm) limestone bedrock at depth, a highly conductive (<10 Ωm) clay layer on top, and, in particular between 200 and 400 m, a layer of intermediate resistivity (~30-100 Ωm), corresponding to the sand banks, and an interbedded strata of clay, sand, and gravel, corresponding to the fluvial deposits.

Probably due to the highly heterogeneous composition of the river delta, these deposits also show a heterogeneous distribution of phase values (Figure 9c). As observed before, the clay and limestone units below the fluvial deposits show low and high phase values, respectively. The relatively high phase values in the clay layer below the fluvial deposits are probably inversion artefacts caused by the relatively noisy TDIP data along this line.

The SRT image (Fig. 9d) shows p-wave velocities as low as 100-200 m/s within the fluvial deposits, which are in agreement with literature values for partially saturated, unconsolidated sand (e.g., Barrière et al., 2012). P-wave velocities increase with depth across the thick (and probably compacted) clay layer. According to the electrical images, the surface of the bedrock lies below the lower limit of the SRT image. Accordingly, the highest velocities of <2000 m/s, seen in the SRT image, do not reach the high values (>2500 m/s) expected for limestone bedrock.

https://doi.org/10.5194/se-2020-75
Preprint. Discussion started: 27 May 2020

5. Discussion

5.1 Sediment-thickness estimation from TEM soundings

The water-borne TEM sounding system set up for this study turned out to provide reliable resistivity images for water depths down to at least 20 m. This conclusion is supported by the good agreement of the resistivity images obtained from water-borne TEM and lake-floor TDIP measurements along both TEM profiles (Fig. 7 and Fig. 9). However, our expectation that the electrically conductive fine-grained sediments could be distinguished from the underlying resistive bedrock turned out to be inappropriate: While the SBP seismograms (and TDIP phase images) lead to the conclusion that the thickness of the fine-grained lakebed sediments does not exceed 5-7 m in Lake Metzabok, conductive units extend down to depths of 20-30 m (below the lake bottom) and more. We resolve this apparent contradiction by postulating an intermediate layer made of limestone debris from collapsed karst cavities and fine-grained sediments filling the spaces between the limestone blocks. This mixed layer seems to be characterized by a much higher seismic velocity compared to the fine sediments but a similar or slightly lower electrical resistivity. Consequently, the small resistivity contrast between the fine-grained lakebed sediments and the underlying mixed layer hinders an unambiguous estimation of sediment thickness from TEM (and TDIP) resistivity data.

It is worth mentioning that previous shallow-water TEM studies (Butler, 2009; and references therein; Hatch et al., 2010; Mollidor et al., 2013) employed in-loop configurations with an outer transmitter loop and a smaller receiver loop or coil in the centre, while we used a single-loop configuration, which is quicker to assemble and easier to handle while navigating on the lake. We also showed that it is sensible to constrain the interpretation of the sounding data by incorporating water depth and eventually water resistivity into the inversion process as a-priori information. Water depth is readily measured during the TEM sounding using a standard echo sounder. Further investigations can consider the addition of fluid conductivity and temperature measurements using conductivity-temperature-depth (CTD) probes to improve the inversion of waterborne measurements and, thus, the investigations of the lake bed by electrical methods. Such information can also be obtained from the analysis of water samples.

5.2 Induced-polarization imaging of the lake floor

Due to the low phase response of the lake sediments and the comparably high response of the limestone bedrock as well as the collapse-debris layer, the phase images obtained from TDIP data measured on the dry lake bottom turned out to be more conclusive for the delimitation of the layer of pure sediments than the resistivity images. We conclude this from the good overall agreement of the shallow low-phase layer with the corresponding reflector in the SBP images.

Although this is definitely an interesting result, the practical relevance of this finding for measurements on water-filled lakes would still have to be tested: In principle, TDIP data could be collected with floating electrode arrays as used for water-borne direct-current resistivity surveys. However, the collection of deep IP data - as needed to investigate the sediments below a

https://doi.org/10.5194/se-2020-75
Preprint. Discussion started: 27 May 2020

water column of, e.g., 20 m – often suffers from a low S/N ratio. This limitation could possibly be overcome by bringing the electrodes closer to the lake bottom.

5.3 Seismic versus electrical surveys

For shallow-water applications, the compact and mobile experimental setup as well as the high productivity and resolution in combination with the straight-forward interpretation of the SBP lead to the conclusion that reflection seismic methods will probably not be substituted by TEM surveys. The latter are by far slower and more labour intensive in the field and in the office, and the resulting imaging results have a lower resolution. However, under the given geological conditions in the study area, waterborne TEM soundings have proven to work well and provide relevant complementary data. In our study, waterborne TEM soundings allowed to delineate the collapse-debris layer between fine-grained lakebed sediments and bedrock.

The situation is different when measurements have to be carried out directly on the bed of a dry lake: There, the muddy surface results in a high energy loss of seismic signals, which considerably decreases the quality of seismic data (as, e.g., reflected by a low picking percentage) and makes the application of SRT methods challenging. At the same time, the low contact resistances and the easy installation of electrodes on the soft ground represent ideal conditions for electrical imaging measurements. Therefore, it is not surprising that both productivity and data quality are higher for TDIP than for SRT measurements. The good agreement of our electrical data with co-located seismic reflection data (SBP), suggests that under certain conditions electrical surveys can eventually replace seismic surveys, especially if phase data is available.

6. Conclusions

Based on field data collected on two karst lakes, the present study investigates the potential and limitations of electrical and electromagnetic geophysical methods for the reconnaissance of the bottom of shallow lakes and their sedimentary infill. The good agreement of electrical resistivity data collected with a water-borne TEM system, TDIP resistivity data collected directly on the dry lake bottom, and electrical measurements on sediment samples in the laboratory demonstrates that the proposed TEM system works well down to water depths of at least 20 m. TDIP phase images turned out to provide relevant complementary information – here, in particular about the inner structure of the conductive units covering the lake bottom. Seismic data from a water-borne SBP and a SRT survey on the dry lake floor provided complementary information and allowed to interpret the two conductive units as a top layer of fine-grained sediments and an intermediate layer of debris from collapsed cavities in the heavily karstified limestone bedrock. At the same time, the delineation of the upper limit of the buried limestone bedrock was not possible from the seismic data only. Thus, the final interpretation was only possible by combining electrical and seismic data sets and by incorporating geological and geomorphological constraints, showing – once again – the strength of a multi-methodological and interdisciplinary approach.

https://doi.org/10.5194/se-2020-75
Preprint. Discussion started: 27 May 2020

Data availability

All raw and processed data of this study (and some additional data not discussed here) are available at Zenodo (https://doi.org/10.5281/zenodo.3782402) along with the Matlab scripts used to prepare the visualizations presented in this manuscript.

Author contributions

AFO, JG, JH, WM, EG, and JR participated in the field seasons, which were planned and coordinated by MB, LP, AFO, CP, AH, and AS. RG and JH were responsible for the sediment and water samples and the laboratory IP data. CP, EG, and JR processed the SBP data. AFO processed and inverted the TDIP data, MS the SRT data, and LA the TEM data. WM made a geological field survey and gave insights into the geological context. JB prepared the maps and participated in the geological contextualization. All authors participated in the interpretation and discussion of the results. MB lead the redaction of the manuscript with contributions of all co-authors.

Competing interests

The authors declare that they have no conflict of interest.

Acknowledgements

We thank the Comisión Nacional de Áreas Naturales Protegidas (CONANP) and the authorities of the protected area Nahá and Metzabok, in particular Sergio Montes Quintero, Santiago Landois Álvarez Icaza, Miguel García Cruz, Rafael Tarano, and José Ángel Solórzano, as well as the municipalities of Nahá and Metzabok for their openness and friendly support. We are grateful for the help provided by Mauricio Bonilla, Johannes Bücker, Martín Garibay, Carlos Cruz, Roberto Reyes, Lorena Bárcena, Rodrigo Martínez Abarca, and Theresia Lauke, and all other colleagues and students, who were actively involved during the field seasons. Finally, we would like to thank Socorro Lozano, Margarita Caballero, Beatriz Ortega, Sergio Rodríguez, and Alex Correa Metrio from the Institutes of Geology and Geophysics, UNAM, for institutional and logistical support.

Financial support

Financial support was provided by Consejo Nacional de Ciencia y Tecnología (CONACyT) under grant number 252148 and Deutsche Forschungsgemeinschaft (DFG) under grant numbers BU3911/1-1 and PE2133/1-1. Parts of this work were funded through the Austrian Science Fund (FWF) – Agence Nationale de la Recherche (ANR) research project FWF-I-2619-N29 and

ANR-15-CE04-0009-01 HYDROSLIDE: Hydro-geophysical observations for an advanced understanding of clayey landslides as well as by the Austrian Federal Ministry of Science, Research and Economy (project: ExploGRAF- Development of geophysical exploration methods for the characterization of mine-tailings towards exploitation).

References

Bairlein, K., Hördt, A., and Nordsiek, S.: The influence on sample preparation on spectral induced polarization of unconsolidated sediments, Near. Surf. Geophys., 12(5), 667-678, https://doi.org/10.3997/1873-0604.2014023, 2014.

Barrière, J., Bordes, C., Brito, D., Sénéchal, P., and Perroud, H.: Laboratory monitoring of P waves in partially saturated sand, Geophys. J. Int., 191(3), https://doi.org/10.1111/j.1365-246X.2012.05691.x, 1152-1170, 2012.

Befus, K. M., Cardenas, M. B., Ong, J. B., and Zlotnik, V. A.: Classification and delineation of groundwater–lake interactions in the Nebraska Sand Hills (USA) using electrical resistivity patterns. Hydrogeology Journal, 20(8), 1483-1495, https://doi.org/10.1007/s10040-012-0891-x, 2012.

Binley, A., and Kemna, A.: DC resistivity and induced polarization methods, in: Hydrogeophysics, edited by Rubin, Y., and Hubbard, S.S., Springer Netherlands, Dordrecht, Netherlands,129–156, https://doi.org/10.1007/1-4020-3102-5_5, 2005.

Bücker, M., Lozano-Garcia. S., Ortega-Guerrero, B., Caballero-Miranda, M., Pérez, L., Caballero, L., Pita de la Paz, C., Sánchez-Galindo, A., Jesús Villegas, F., Flores Orozco, A., Brown, E., Werne, J., Valero Garcés, B., Schwalb, A., Kemna, A., Sánchez-Alvaro, E., Launizar-Martínez, N., Valverde-Placencia, A., and Garay-Jiménez, F.: Geoelectrical and Electromagnetic Methods Applied to Paleolimnological Studies: Two Examples from Desiccated Lakes in the Basin of Mexico, B. Soc. Geol. Mex., 69(2), 279-298, http://dx.doi.org/10.18268/bsgm2017v69n2a1, 2017.

Butler, K. E.: Trends in waterborne electrical and EM induction methods for high resolution sub-bottom imaging, Near. Surf. Geophys., 7(4), 241-246, https://doi.org/10.3997/1873-0604.2009002, 2009.

Cohen, A. S.: Paleolimnology: the history and evolution of lake systems, Oxford University Press, New York, USA, 528 pp., 2003.

Cohuo, S., Macario-González, L., Pérez, L., Sylvestre, F., Paillès, C., Curtis, J. H., Kutterolf, S., Wojewódka, M., Zawisza, E., and Schwalb, A.: Climate ultrastructure and aquatic community response to Heinrich Stadials (HS5a-HS1) in the continental northern Neotropics, Quaternary Sci. Rev. 197, 75-91., https://doi.org/10.1016/j.quascirev.2018.07.015, 2018.

Colombero, C., Comina, C., Gianotti, F., and Sambuelli, L.: Waterborne and on-land electrical surveys to suggest the geological evolution of a glacial lake in NW Italy, J. Appl. Geophys., 105, 191-202, https://doi.org/10.1016/j.jappgeo.2014.03.020, 2014.

Dahlin, T., Leroux, V., and Nissen, J.: Measuring techniques in induced polarisation imaging, J. Appl. Geophys., 50(3), 279-298, https://doi.org/10.1016/S0926-9851(02)00148-9, 2002.

Díaz, K. A., Pérez, L., Correa-Metrio, A., Franco-Gaviria, J. F., Echeverría, P., Curtis, J., and Brenner, M.: Holocene environmental history of tropical, mid-altitude Lake Ocotalito, México, inferred from ostracodes and non-biological indicators, The Holocene 27, 1308-1317, https://doi.org/10.1177/0959683616687384, 2017.

Dondurur, D.: Acquisition and processing of marine seismic data, Elsevier, Netherlands, United Kingdom, United States, 606 pp., https://doi.org/10.1016/C2016-0-01591-7, 2018.

Flores Orozco, A., Gallistl, J., Bücker, M., and Williams, K. H.: Decay curve analysis for data error quantification in time-domain induced polarization imaging, Geophysics, 83(2), E75-E86, https://doi.org/10.1190/geo2016-0714.1, 2018.

García-Gil, J.G., and Lugo Hupb, J.: Las formas del relieve y los tipos de vegetación en la Selva Lacandona. in: Reserva de la Biósfera Montes Azules, Selva Lacandona: Investigación para su conservación, edited by: Vásquez-Sánchez, M.A., and Ramos Olmos, M. A., Centro de Estudios para la Conservación de los Recursos Naturales, San Cristóbal de las Casas, Mexico, 39-49, 1992.

Hatch, M., Munday, T., and Heinson, G.: A comparative study of in-river geophysical techniques to define variations in riverbed salt load and aid managing river salinization, Geophysics, 75(4), WA135-WA147, https://doi.org/10.1190/1.3475706, 2010.

Kaufman, A. A., Alekseev, D., Oristaglio, M.: Principles of electromagnetic methods in surface geophysics, 45, Elsevier, Amsterdam, Netherlands, 770 p, 2014.

Kemna, A.: Tomographic inversion of complex resistivity - theory and application, Ph.D., Ruhr-University of Bochum, Bochum, Germany, 176 pp., 2000.

Kemna, A., E. Räkers, and Dresen, L..: Field applications of complex resistivity tomography, in: 69th Annual International Meeting, SEG, Expanded Abstracts, Houston, United States, 31 November – October 31 1999, 331–334, https://doi.org/10.1190/1.1821014, 1999.

Kozola, S.: Large Data in MATLAB: A Seismic Data Processing Case Study, MATLAB Central File Exchange, https://www.mathworks.com/matlabcentral/fileexchange/30585-large-data-in-matlab-a-seismic-data-processing-case-study, 2011.

Kruschwitz, S.: Assessment of the complex resistivity behavior of salt affected building materials, Ph.D., Technical University of Berlin, Berlin, Germany, https://doi.org/10.14279/depositonce-1722, 2007.

Last, W.M., and Smol, J. P.: An introduction to basin analysis, coring and chronological techniques used in paleolimnology, in: Tracking Environmental Change Using Lake Sediments. Developments in Paleoenvironmental Research, edited by: W.M., Smol J. P., Springer, Dordrecht, Netherlands, 1–5, https://doi.org/10.1007/0-306-47669-X_1, 2002.

Lozada Toledo, J.: Usos del agua entre los lacandones de Metzabok, Ocosingo, Chiapas. Un análisis de Ecología Histórica, M.S., El Colegio de la Frontera Sur, San Cristobal de las Casas, Chiapas, Mexico, 261 pp., 2013.

Lozano-García, S., Brown, E. T., Ortega, B., Caballero, M., Werne, J., Fawcett, P. J., Schwalb, A., Valero-Garcés, B., Schnurrenberger, D., O´Grady, R., Stockhecke, M., Steinman, B., Cabral-Cano, E., Caballero, C., Sosa-Nájera, S., Soler, A. M., Pérez, L., Noren, A., Myrbo, A., Bücker, M., Wattrus, N., Arciniega, A., Wonik, T., Watt, S., Kumar, D., Acosta, C.,

https://doi.org/10.5194/se-2020-75
Preprint. Discussion started: 27 May 2020

Martínez, I., Cossio, R., Ferland, T., Vergara-Huerta, F.: Perforación profunda en el lago de Chalco: reporte técnico, B. Soc. Geol. Mex. 69, 299-311, http://dx.doi.org/10.18268/bsgm2017v69n2a2, 2017.

Mandujano-Velazquez, J. J., and Keppie, J. D.: Middle Miocene Chiapas fold and thrust belt of Mexico: a result of collision of the Tehuantepec Transform/Ridge with the Middle America Trench. Geol. Soc. Spec. Publ. 327(1), 55-69, https://doi.org/10.1144/SP327.4, 2009.

Mollidor, L., Tezkan, B., Bergers, R., and Löhken, J.: Float-transient electromagnetic method: in-loop transient electromagnetic measurements on Lake Holzmaar, Germany. Geophysical Prospecting, 61(5), 1056-1064, https://doi.org/10.1111/1365-2478.12025, 2013.

Orlando, L.: Some considerations on electrical resistivity imaging for characterization of waterbed sediments, J. Appl. Geophys., 95, 77-89, https://doi.org/10.1016/j.jappgeo.2013.05.005, 2013.

Pelton, W. H., Ward, S. H., Hallof, P. G., Sill, W. R., and Nelson, P. H.: Mineral discrimination and removal of inductive coupling with multifrequency IP, Geophysics, 43(3), 588-609, https://doi.org/10.1190/1.1440839, 1978.

Pérez, L., Bugja, R., Lorenschat, J., Brenner, M., Curtis, J., Hoelzmann, P., Islebe, G., Scharf, B., and Schwalb, A.: Aquatic ecosystems of the Yucatán Peninsula (Mexico), Belize, and Guatemala, Hydrobiologia 661, 407–433, https://doi.org/10.1007/s10750-010-0552-9, 2011.

Reynolds, J. M.: An introduction to applied and environmental geophysics, John Wiley and Sons, Oxford, United Kingdom, 710 pp., 2011.

Rubio Sandoval, C. Z.: Estudio paleoambiental en dos lagos kársticos de la Selva Lacandona, Chiapas, Mexico, durante los últimos ~500 años utilizando indicadores biológicos y geoquímicos, M.S., Universidad Nacional Autónoma de México, Mexico City, Mexico, 117 pp., 2019.

Rücker, C., Günther, T., Wagner, F. M.: pyGIMLi: An open-source library for modelling and inversion in geophysics, Computers and Geosciences, 109, 106-123, https://doi.org/10.1016/j.cageo.2017.07.011, 2017.

Schindler, D.W.: Lakes as sentinels and integrators for the effects of climate change on watersheds, airsheds, and landscapes, Limnol. Oceanogr., 54(6), 2349, https://doi.org/10.4319/lo.2009.54.6_part_2.2349, 2009.

Scholz, C. A.: Applications of seismic sequence stratigraphy in lacustrine basins, in: Tracking Environmental Change Using Lake Sediments. Developments in Paleoenvironmental Research, edited by: W.M., Smol J. P., Springer, Dordrecht, Netherlands, 7–22, https://doi.org/10.1007/0-306-47669-X_2, 2002.

Sigala, I., Caballero, M., Correa-Metrio, A., Lozano-García, S., Vázquez, G., Pérez, L., and Zawisza, E.: Basic limnology of 30 continental waterbodies of the Transmexican Volcanic Belt across climatic and environmental gradients, B. Soc. Geol. Mex. 69, 313–370, http://dx.doi.org/10.18268/bsgm2017v69n2a3, 2017.

Toran, L., Nyquist, J., Rosenberry, D., Gagliano, M., Mitchell, N., and Mikochik, J.: Geophysical and hydrologic studies of lake seepage variability, Groundwater, 53(6), 841-850, https://doi.org/10.1111/gwat.12309, 2015.

Uyanık, O.: The porosity of saturated shallow sediments from seismic compressional and shear wave velocities, J. Appl. Geophys., 73(1), 1, https://doi.org/10.1016/j.jappgeo.2010.11.001, 2011.

https://doi.org/10.5194/se-2020-75
Preprint. Discussion started: 27 May 2020

Van Voorhis, G. D., Nelson, P. H., and Drake, T.L.: Complex resistivity spectra of porphyry copper mineralization, Geophysics, 38(1), 49-60, https://doi.org/10.1190/1.1440333, 1973.

Waxman, M. H., and Smits, L. J. M.: Electrical conductivities in oil-bearing shaly sands, Soc. of Petrol. Eng. J., 8(02), 107-122, https://doi.org/10.2118/1863-A, 1968.

White, D. J.: Two-dimensional seismic refraction tomography, Geophys. J. Int., 97(2), 223-245, https://doi.org/10.1111/j.1365-246X.1989.tb00498.x, 1989.

Table 1: Ranges of physical properties of the geological units interpreted from our geophysical profiles and laboratory measurements. Resistivity data based on TEM, TDIP resistivity and laboratory measurements; phase data (absolute value) according to TDIP images and laboratory data between 1 und 10 Hz; p-wave velocity from SRT images.

Material / geological unit	Resistivity (Ωm)	Phase (mrad)	P-wave velocity (m/s)
Fine-grained sediments	10-30	<4	200-1500
Collapse debris & fine-grained sediments	10-20	>5-6	1500-2000
Limestone bedrock	>100	>4-5	>2000

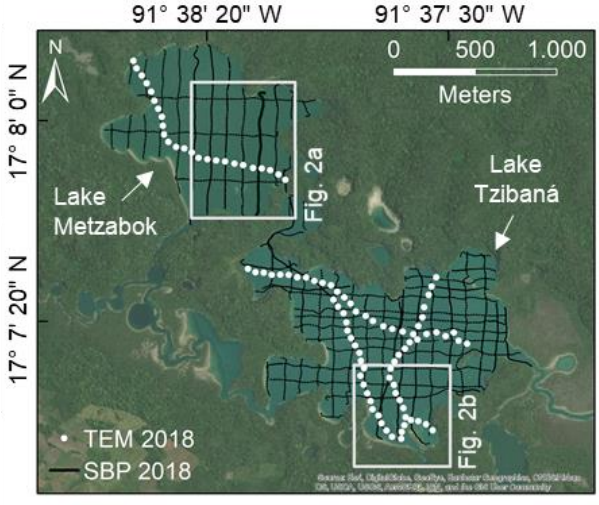

Figure 1: Layout of the geophysical survey on lakes Metzabok and Tzibaná during high-level stands in March 2018. Black lines show the sub-bottom profiler (SBP) survey grid, white circles represent individual transient electromagnetic soundings (TEM). The optical satellite image in the background (source: Bing Maps data base) shows lake water surface similar to the high-level stands encountered during March 2018.

https://doi.org/10.5194/se-2020-75
Preprint. Discussion started: 27 May 2020

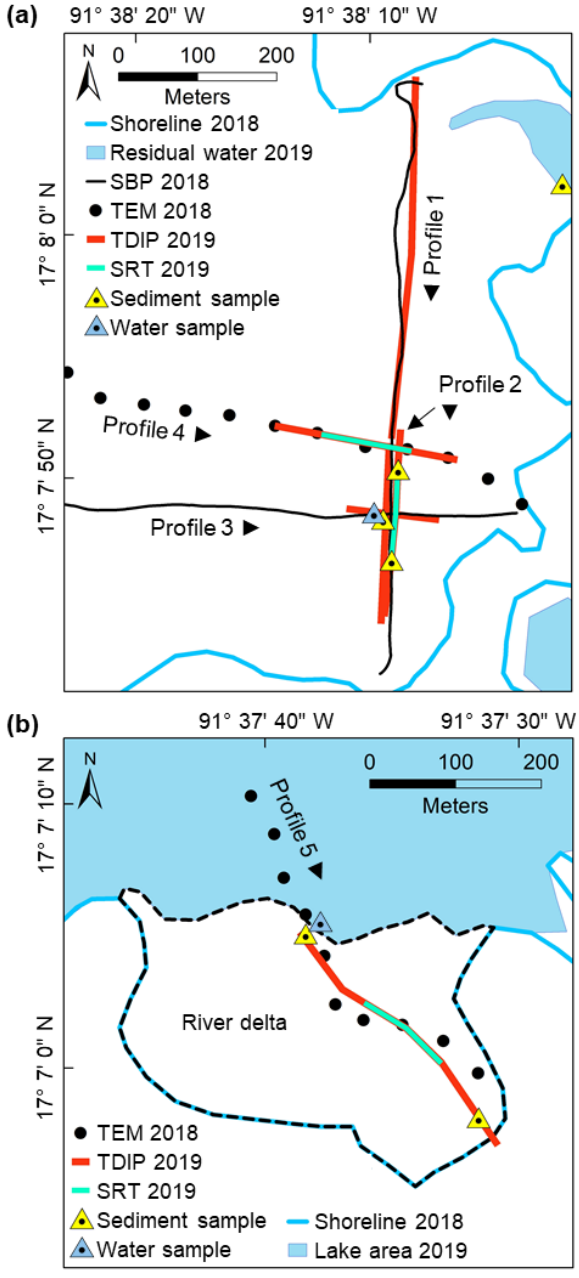

Figure 2: Layout of the geophysical survey on lakes Metzabok (a) and Tzibaná (b) in October 2019 (after the sudden lake-level drop) including sub-bottom profiler (SBP), transient electromagnetic (TEM), time-domain induced polarization (TDIP), and seismic refraction tomography (SRT) measurements. The geophysical measurements discussed here are grouped into five profiles; black triangles next to the profile names indicate the profile orientations. Yellow and blue triangles indicate sampling locations for sediment and water samples analysed in the laboratory, respectively. The dashed black line in (b) indicates the dry part of the river delta exposed during October 2019.

https://doi.org/10.5194/se-2020-75
Preprint. Discussion started: 27 May 2020

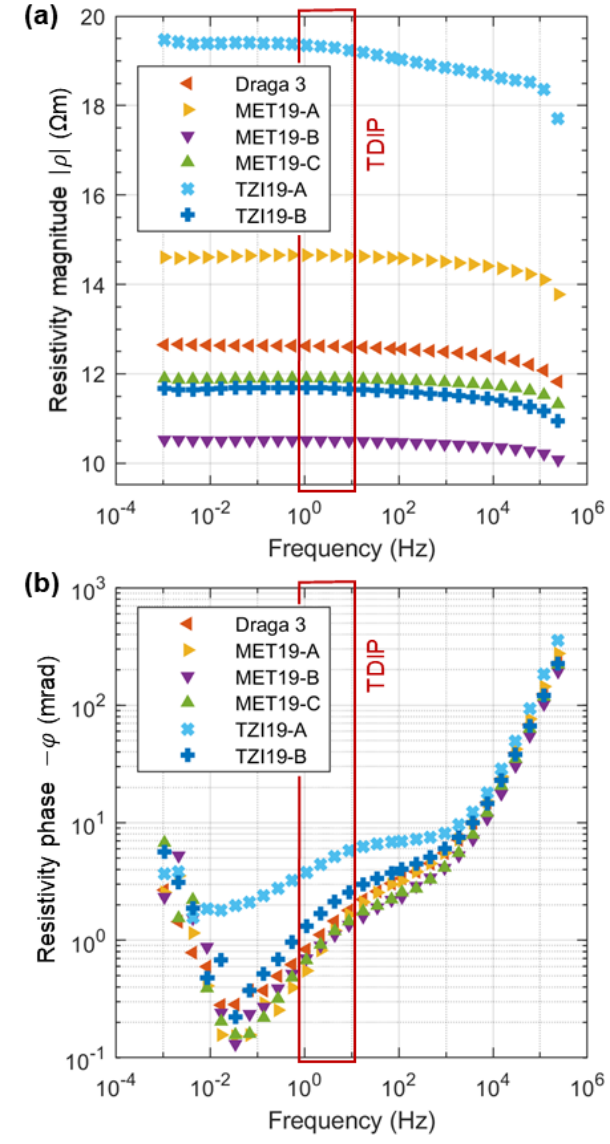

Figure 3: Frequency-dependent complex resistivity of six lake-bottom sediment samples retrieved from Lake Metzabok (triangles) and Lake Tzibaná (crosses). Complex-resistivity values are given in terms of (a) magnitude and (b) phase. The highlighted frequencies between 1 and 10 Hz roughly correspond to the range tested by our time-domain induced polarization measurements in the field.

https://doi.org/10.5194/se-2020-75
Preprint. Discussion started: 27 May 2020

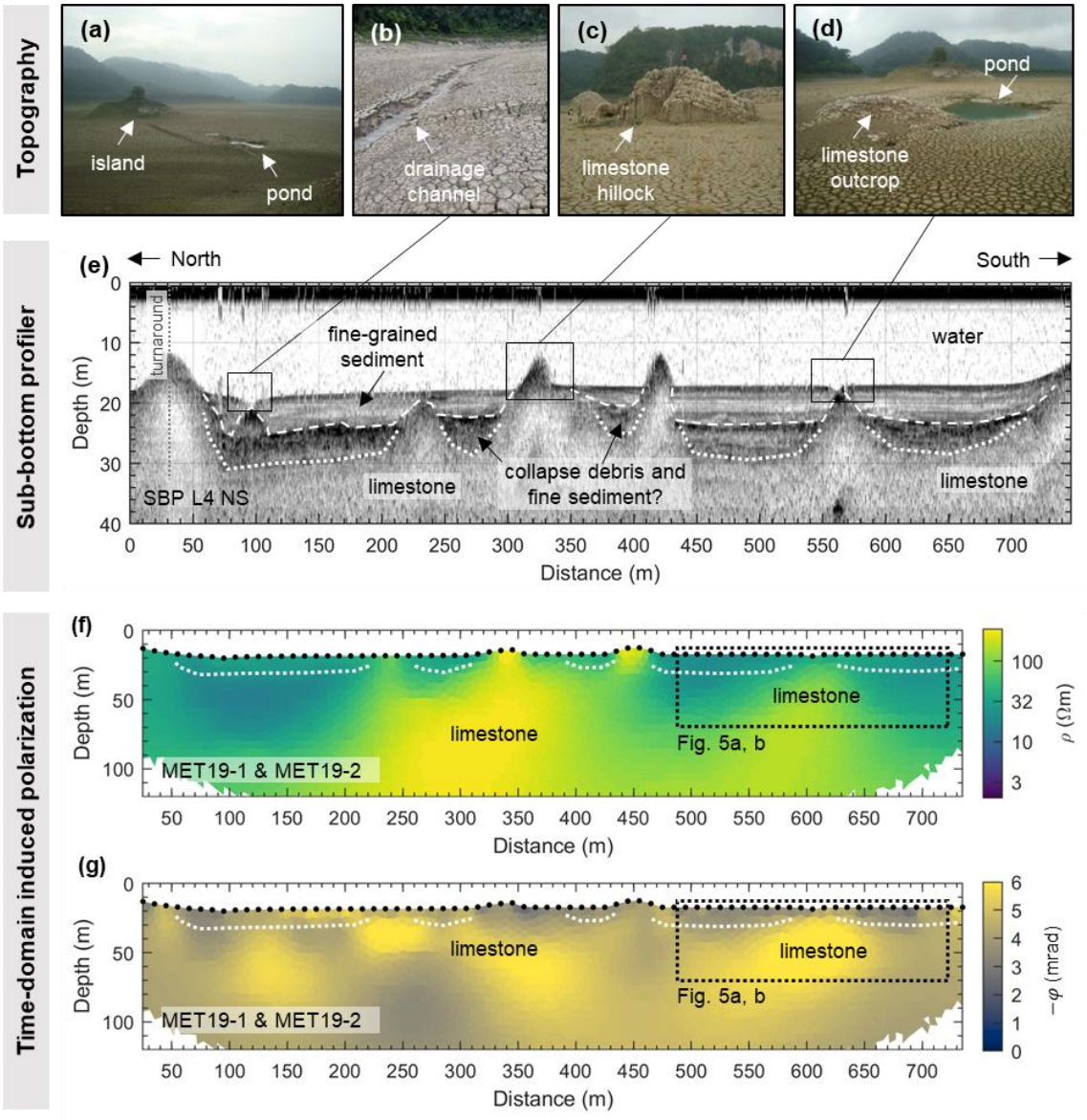

Figure 4: Topographic features and geophysical sections along Profile 1 of Lake Metzabok. Photographs of topographical features taken in October 2019: (a) lake basin with flat bottom, (b) drainage channel, (c) limestone hillock, (d) deep fracture and pond next to shallow limestone outcrop. (e) sub-bottom profiler section with dashed lines highlighting the main reflector encountered below the lake floor and dotted lines outlining a zone of high diffuse reflectivity, (f) and (g) electrical resistivity and phase images, respectively, including electrode positions (black dots along the surface) and dotted lines taken from SBP section. Labels in the lower left corners of the sections refer to the IDs within the data set published along this manuscript.

https://doi.org/10.5194/se-2020-75
Preprint. Discussion started: 27 May 2020

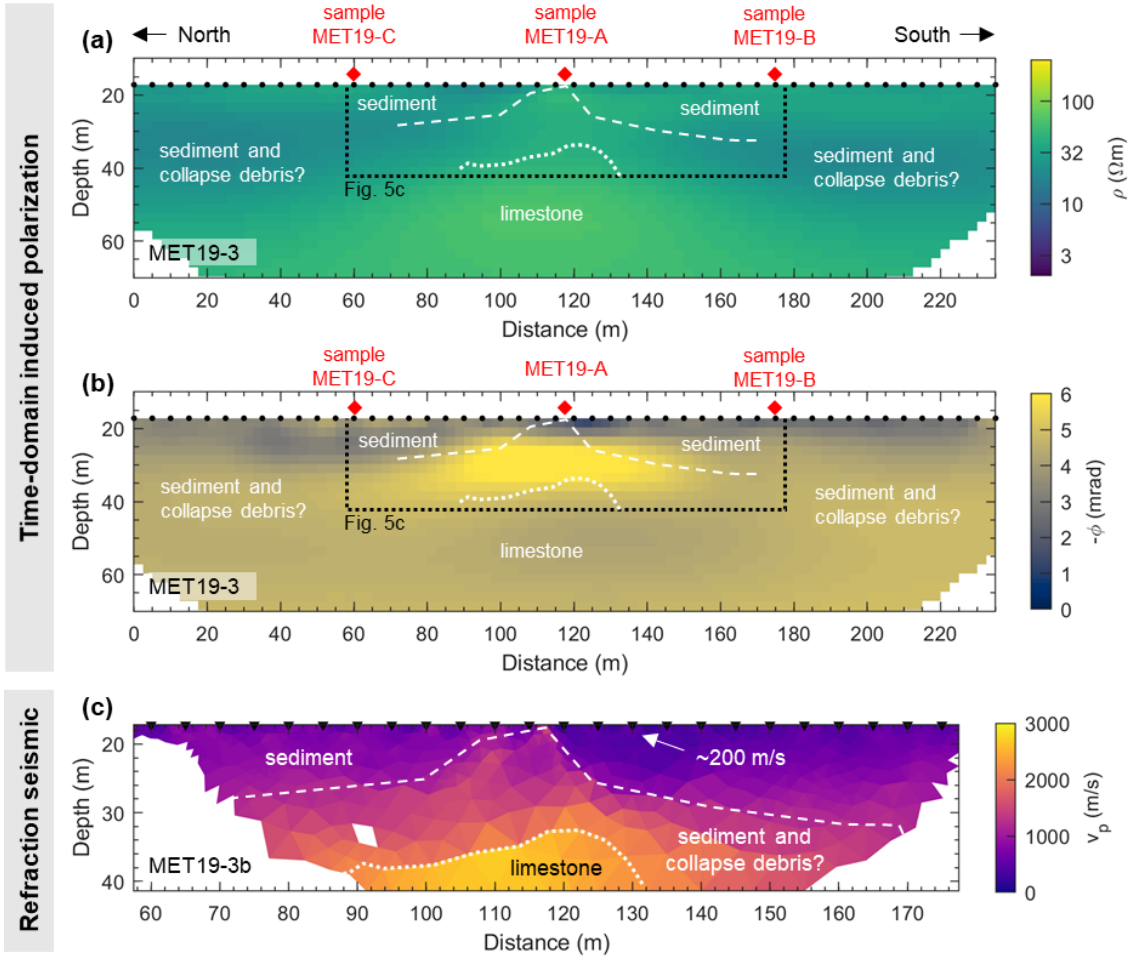

Figure 5: Geophysical sections along Profile 2 of Lake Metzabok: (a) and (b) electrical resistivity and phase images, respectively, including electrode positions (black dots along the surface), sampling locations of sediment samples (red diamonds at the surface), and the main lithological units interpreted from the SBP image (dotted lines); (c) seismic refraction tomogram with main lithological units. Labels in the lower left corners of the sections refer to the IDs within the data set published along this manuscript.

https://doi.org/10.5194/se-2020-75
Preprint. Discussion started: 27 May 2020

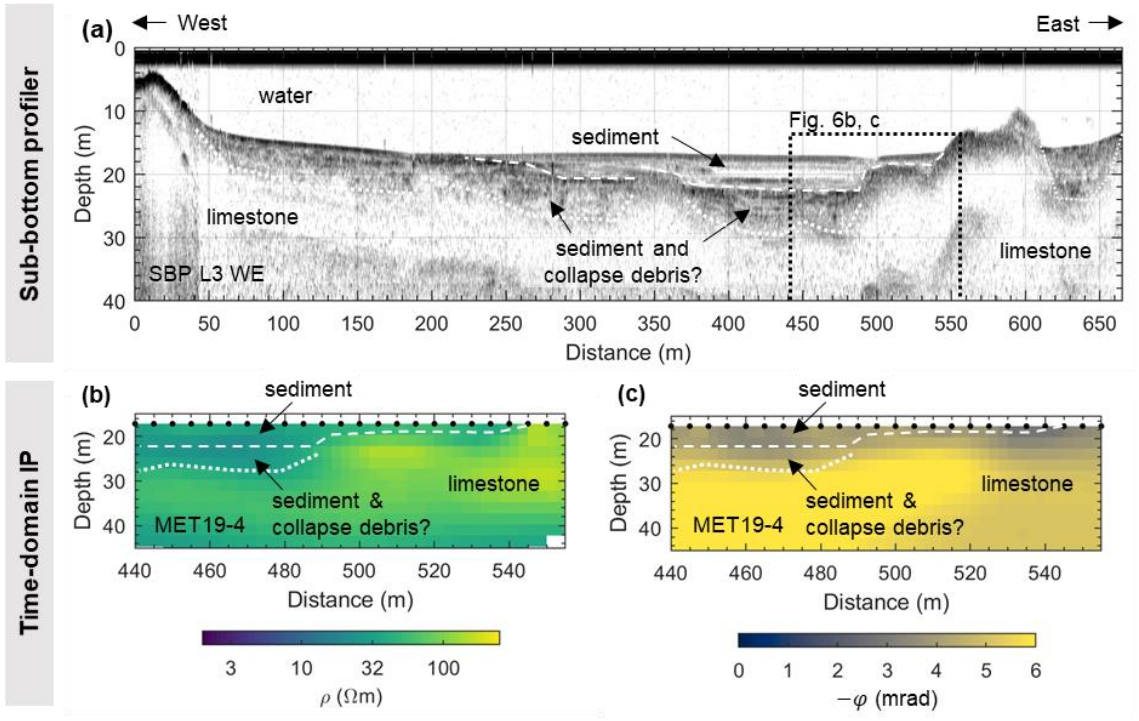

Figure 6: Geophysical sections along Profile 3 of Lake Metzabok: (a) sub-bottom profiler section with dashed lines highlighting the main reflector found below the lake floor, dotted lines outlining a zone of high diffuse reflectivity including main reflectors and the dashed box showing the section with ERT/IP data, (b) electrical-resistivity image and (c) phase image including electrode positions (black dots along the surface) and lines taken from SBP seismogram. Labels in the lower left corners of the sections refer to the IDs within the data set published along this manuscript.

https://doi.org/10.5194/se-2020-75
Preprint. Discussion started: 27 May 2020

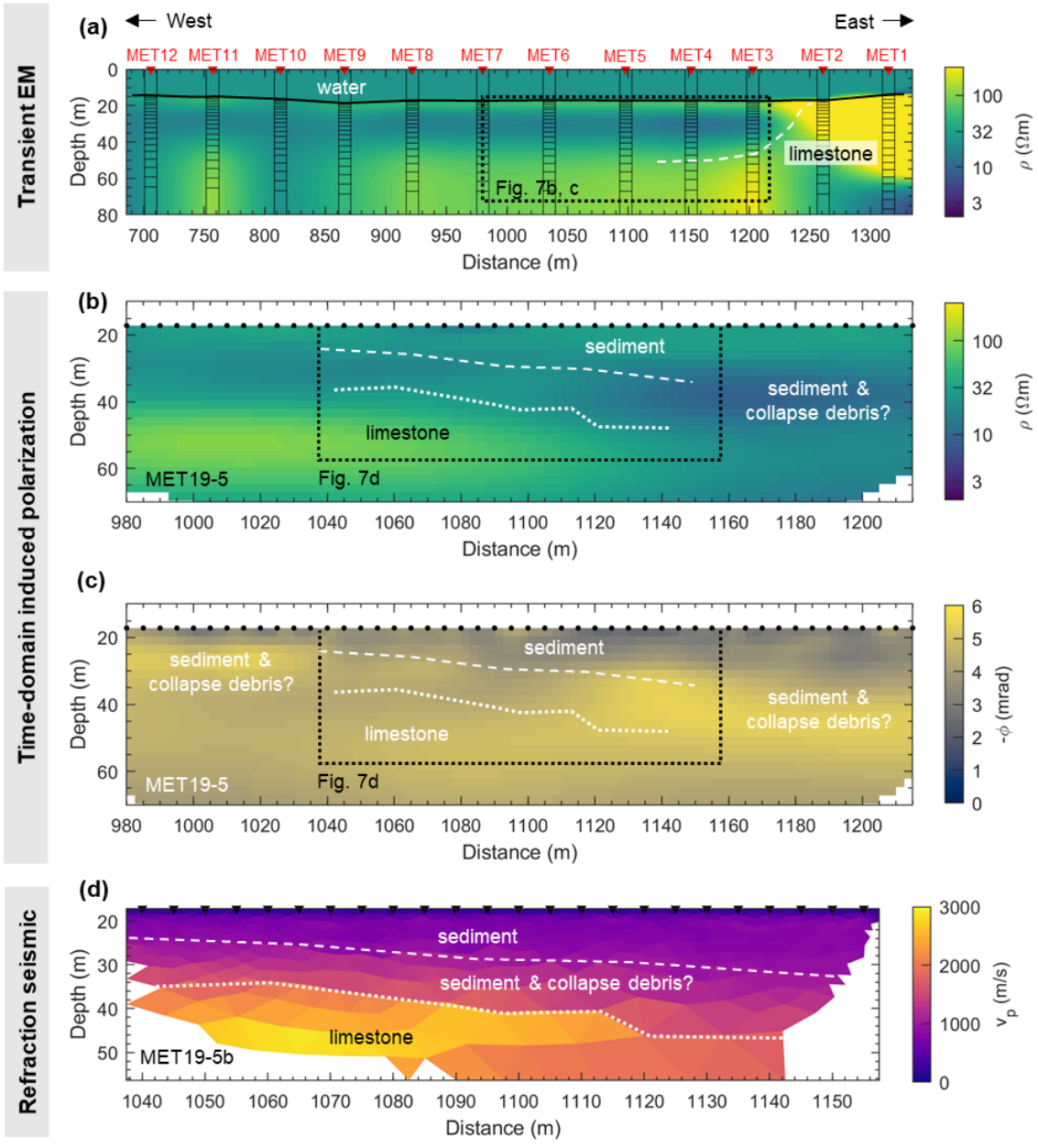

Figure 7: Geophysical sections along Profile 4 of Lake Metzabok: (a) TEM image based in smooth 1D models (bar graphs in the foreground) and interpolated 2D section (background); the black solid line indicates the water-sediment contact, the dashed line the inferred geometry of the limestone bedrock. (b) electrical resistivity and (c) phase images including electrode positions (black dots along the surface), and the main lithological units as interpreted from the SRT image in (d) (dotted lines); (d) seismic refraction tomogram with main lithological units. Labels in the lower left corners of the sections refer to the IDs within the data set published along this manuscript.

https://doi.org/10.5194/se-2020-75
Preprint. Discussion started: 27 May 2020

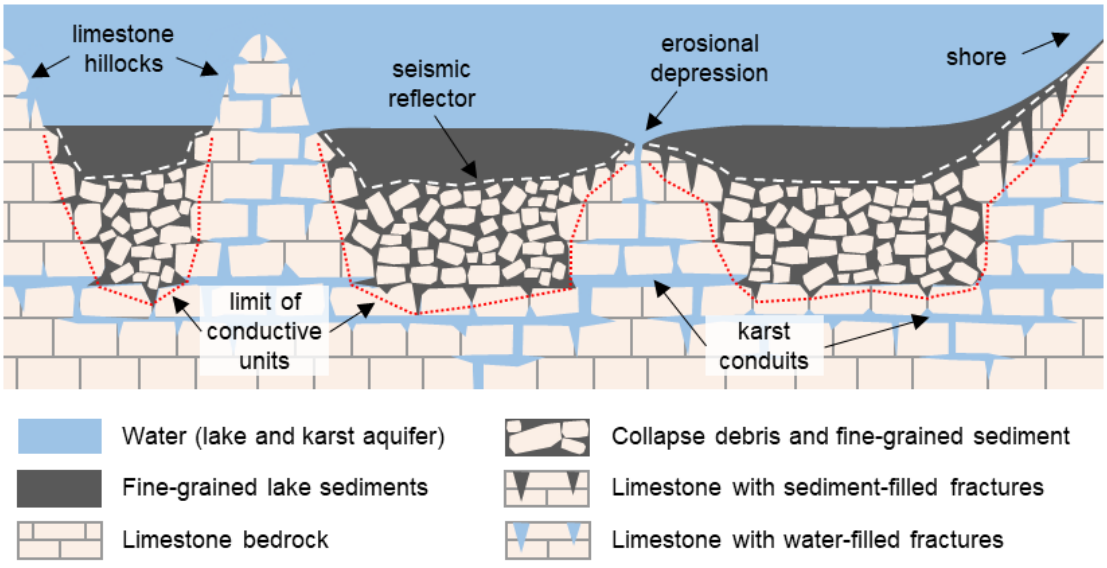

Figure 8: Schematic sketch summarizing the geological conditions below Lake Metzabok interpreted from the geophysical survey (details not drawn to scale). The limit between the fine-grained lake sediments and the collapse debris with sediment-filled interspaces indicated by the white dashed line stands out as a strong reflector in all sub-bottom profiler images. All units containing fine-grained sediment are characterized by low electrical resistivity values; a strong resistivity increase marks the upper limit of the limestone bedrock as indicated by the red dotted line.

https://doi.org/10.5194/se-2020-75
Preprint. Discussion started: 27 May 2020

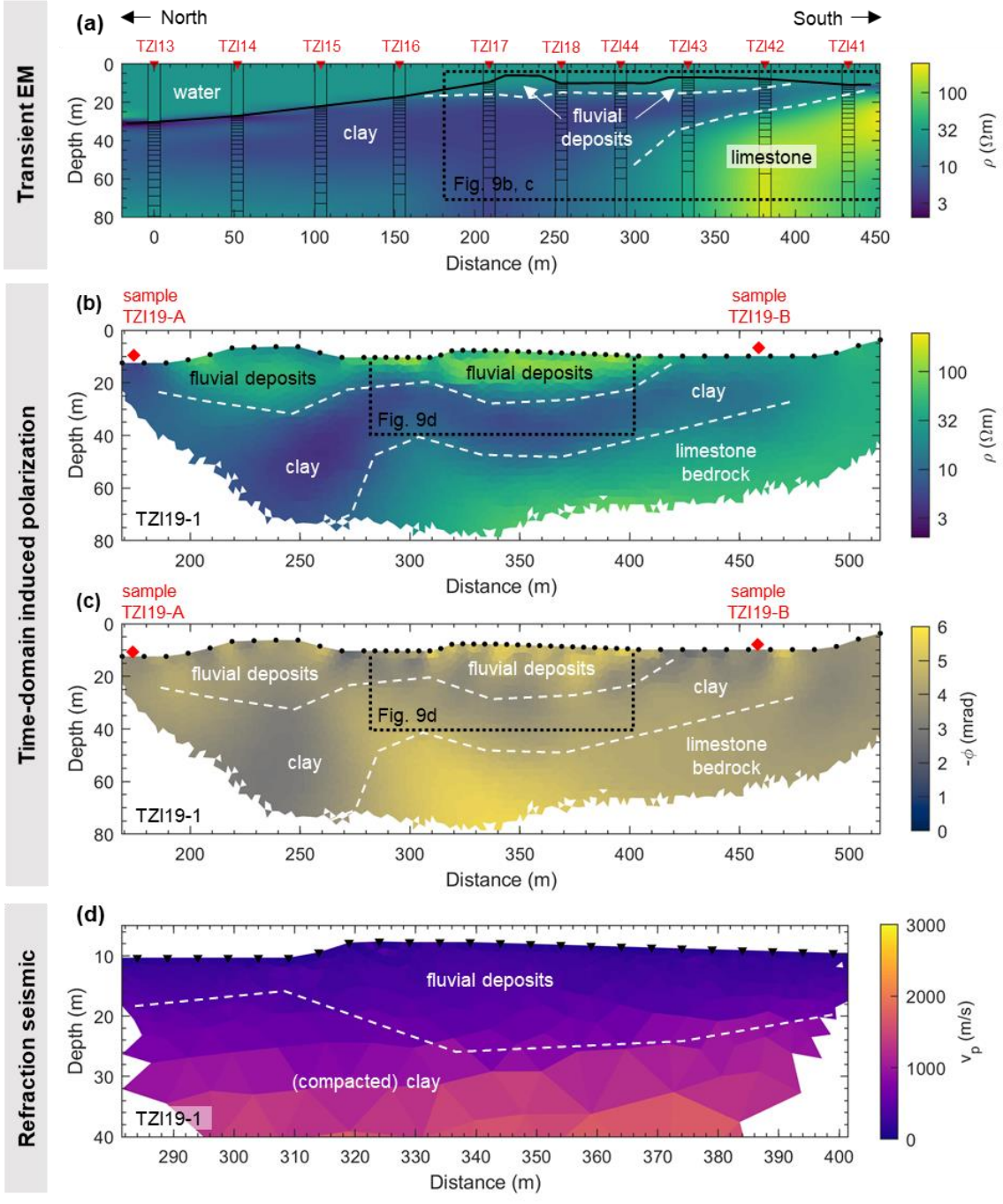

Figure 9: Geophysical sections along Profile 5 of Lake Tzibaná: (a) TEM image based on smooth 1D models (bar graphs in the foreground) and interpolated 2D section (background); the black solid line indicates the water-sediment contact, the dashed line the main lithological contacts inferred from this image; (b) electrical resistivity and (c) phase images including electrode positions (black dots along the surface) and main lithological units. Red diamonds on the surface indicate the location of the sediments sampled for laboratory analyses; (d) seismic refraction tomogram including the contact between fluvial deposits and clay taken from the TDIP resistivity image. Labels in the lower left corners of the sections refer to the IDs within the data set published along this manuscript.